Journal of Power Sources 196 (2011) 9008–9012

Contents lists available at ScienceDirect

Journal of Power Sources

journal homepage: www.elsevier.com/locate/jpowsour

Short communication

Microplasma reforming of hydrocarbons for fuel cell power

R.S. Besser*, P.J. Lindner

Department of Chemical Engineering and Materials Science, Stevens Institute of Technology, Castle Point on Hudson, Hoboken, NJ 07030, United States

ARTICLE INFO

Article history:
Received 29 October 2010
Received in revised form
17 November 2010
Accepted 23 November 2010
Available online 1 December 2010

Keywords:
Microplasma
Plasma
Micro hollow cathode discharge
Fuel reforming
Fuel cell
Hydrogen

ABSTRACT

The implementation of a microplasma approach for small scale reforming processes is explored as an alternative to more standard catalyst-based processes. Plasmas are a known approach to activating a chemical reaction in place of catalysts, and microplasmas are particularly attractive owing to their extremely high electron and power densities. Their inherent compactness gives them appeal for portable applications, but their modularity leads to scalability for higher capacity. We describe the realization of experimental microplasma reactors based on the microhollow cathode discharge (MHCD) structure by silicon micromachining for device fabrication. Experiments were carried out with model hydrocarbons methane and butane in the reactors within a microfluidic flow and analytical setup. We observe several key phenomena, including the ability to liberate hydrogen from the hydrocarbons at temperatures near ambient and sub-Watt input power levels, the tendency toward hydrocarbon decomposition rather than oxidation even in the presence of oxygen, and the need for a neutral carrier to obtain conversion. Mass and energy balances on these experiments revealed conversions up to nearly 50%, but the conversion of electrical power input to chemical reaction enthalpy was only on the order of 1%. These initial, exploratory results were recorded with devices and at process settings without optimization, and are hence promising for an emerging, catalyst-free reforming approach.

1. Introduction

While the pace at which new devices powered by electrical energy seem to grow exponentially, the technology for long lived, robust, and cost-effective power sources to energize them has not kept pace. While this is typified by the soldier whose main payload consists of batteries to power all his/her electronic devices, the picture is the same for the civilian carrying multiple devices for communicating, organizing, and creating. Small hydrogen powered fuel cells have been viewed as the logical successor to the battery for portable power for some time [1], but this potential has not been realized, due mostly to the problem of a high density source for hydrogen with satisfactory reliability and lifetime. Direct methanol and similar fuel cell approaches are excluded because of their weaker performance limited by fuel crossover. The most logical approach to the need seems to be through the conversion of hydrocarbon fuels because of their high specific energy density compared to the alternative of compressed hydrogen. While reforming of these fuels by catalytic processes has been shown to be scalable [2,3], there has yet to be established a process with the reliability, performance, and compactness [4] required to drive commercial application.

The key limitation of the catalytic approaches is imposed by the catalysts themselves. Catalysts in hydrocarbon conversion are subjected to conditions which can neutralize their effectiveness by various mechanisms. Deposition of carbon, known as coking, can occur on the active sites of the catalyst rendering them ineffective. Other contaminants found in hydrocarbon fuels, notably sulfur, can poison active sites, eliminating their activity. Additionally, many catalytic reforming processes must be carried out at relatively high temperatures (>600 °C) that eventually cause catalysts to agglomerate, reducing available surface area and active site density. Moreover, these temperatures put a constraint on the type of materials of construction of the reformer, resulting in higher costs and complexity.

The primary appeal of microplasma reforming is in the elimination of all these issues by avoiding catalysts altogether and instead using the plasma to activate the reaction. The microplasma environment is rich in charged species, neutrals, and reactive radicals and thus can vigorously promote reaction [5–7]. The notion of the plasma as an enabling environment for reforming of hydrocarbons is not new as exemplified by the review paper of Petitpas et al. [8] and elsewhere [9–11]. However, microplasmas, generated in sub-mm geometry, such as the MHCD devices presented here, have unique properties over against more conventionally generated plasmas.

The microplasmas presented operate at atmospheric pressure and consequently possess the potential for a much higher plasma density than conventional industrially produced plasmas that most

* Corresponding author. Tel.: +1 201 216 5257; fax: +1 201 216 8306.
E-mail address: rbesser@stevens.edu (R.S. Besser).

0378-7753/$ – see front matter © 2010 Elsevier B.V. All rights reserved.
doi:10.1016/j.jpowsour.2010.11.135

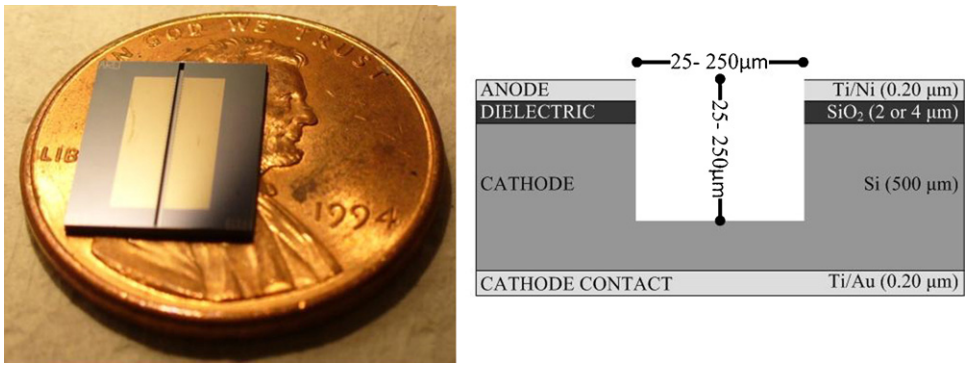

Fig. 1. Illustration of microplasma reactor chip in relation to US one cent coin (left). Schematic cross-section of microplasma reactor chip showing key layers and critical dimensions of the device.

frequently operate at reduced pressure. The densities produced in MHCD structures have exceeded 10^{15} cm^{-3} in electron density [12,13], a value which is at least four orders of magnitude higher than reduced pressure plasmas in semiconductor etching systems. Moreover, the electron energy density function possesses a significant fraction of electrons with energies exceeding 5 eV [12,14], which surpasses the bond energies in hydrocarbons, facilitating reaction. Consequently, the microplasma is not simply a downscaling of conventional plasma reactors, it in fact opens up new opportunities for processing based on favorable attributes that arise from miniaturization. An individual unit microplasma reactor could form the basis of a reformer in a compact energy production system in the sub-Watt range. However, scaling is possible by a multiplicative assembly of units, sometimes referred to as "numbering up" in the microchemical system literature [3].

2. Materials and methods

2.1. Fabrication of microplasma reactors

The basic structure of the device is shown in cross section in Fig. 1. The key fabrication challenge is in creating the vertical walled, high aspect ratio channel which forms the hollowed region in the conductive silicon cathode. This is accomplished through deep reactive ion etching of silicon, a technique popularized for microelectromechanical system (MEMS) fabrication [15].

The fabrication process begins with highly doped silicon wafers, 100 mm in diameter. High temperature oxidation yields a quality SiO_2 dielectric layer which serves to insulate anode from cathode with sufficiently high standoff voltage to tolerate the high potentials needed to achieve plasma formation. The thickness of the SiO_2 was made either 2 μm or 4 μm thick to experimentally observe the effects of varying electric field intensity. After forming the dielectric layer, the anode metallization was created using lift-off lithography and deposition of Ni with a Ti adhesion layer. Pertinent device geometries are labeled in Fig. 1.

The channel was then patterned by photolithography and dry etching applied to etch through the dielectric and then into the silicon. A layer of Ti/Au was evaporated on the back to provide a low resistance cathode contact. After separation of the wafer into individual reactor chips, reaction tests were carried out.

2.2. Reaction testing setup

An individual microplasma reactor chip is loaded into the chip carrier (Fig. 2, left) which connects into the rest of the testing setup as shown in the schematic layout in Fig. 2 (right). High purity reactant gases are fed through mass flow controllers (Aalborg, Inc.) to provide a stable feed to the chip. The reactor chip is powered by either a digitally controlled high voltage DC power supply (Stanford Research Systems, Inc.) or a pulsed DC supply which incorporates a function generator (Wavetek, Inc.) to control the output. Voltage and current supplied to the reactor chip are monitored by an A/D interface circuit connected via a USB port.

Analytical instrumentation consisted of a Varian CP-4900 micro gas chromatograph and a Stanford Research Systems 200 AMU quadrupole mass spectrometer. Two separate columns in the CP-4900 with different affinities were used to expand the sensitivity of the GC measurement.

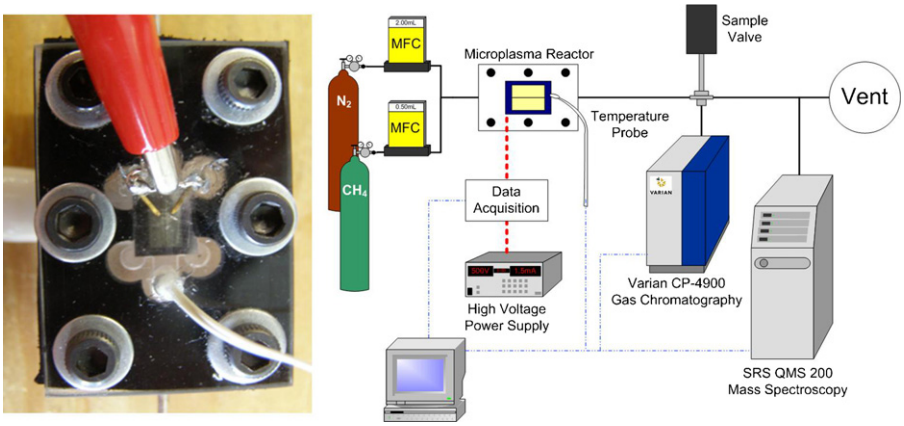

Fig. 2. Microplasma reactor chip inside sealed chip holder during reaction experiment (left). Schematic of reaction characterization setup (right). Solid lines denote fluidic connections, heavy dashed lines denote high-voltage connection, and light dashed lines denote data interface connection.

A resistive thermal device (RTD) temperature sensor was mounted adjacent to the chip in the outlet flow side of the chip carrier. A simple convective heat transfer calculation based on geometry and flow rates showed that the RTD provides a reading within a degree of the chip temperature. The RTD sensor was adopted over a thermocouple as it provided greater noise immunity. All key data were collected through the A/D interface, facilitating analysis of the reaction data.

The feed hydrocarbon for the experiments described here was methane. Methane was either tested alone, with neutral pure carrier gases (nitrogen, argon, or helium), or with a gas mixture containing oxygen, usually air. However in the present experiments (Section 3), only pure nitrogen was used as the carrier.

The chip carrier was not thermally insulated from the ambient, but was able to freely exchange heat with it. No external heating was applied. Any heating effects came about from the electrical energy input for the plasma.

3. Results

Several key findings came out of the detailed reaction testing. The first of these is that pure hydrocarbon fed to the microplasma reactor experienced no reaction under the conditions accessible in our experiments. Despite the formation of stable plasma, no product species appeared in the analytical spectra and no consumption of fuel was observed. However, the situation changed very quickly with the simple introduction of a neutral carrier gas, such as nitrogen, with reaction proceeding immediately as evidenced by the production of hydrogen.

From the distribution of products, it is apparent that decomposition is the preferred mode of reaction, even in the presence of oxidizing species. For example, when air is introduced as the carrier, hydrogen is produced; however, oxides of carbon appear in only low concentrations, well below levels for stoichiometric oxidation. In addition, particulate carbon deposits have been observed on the upper anode surfaces that are exposed to the plasma. This evidence for the production of elemental carbon is consistent with conversion dominated by hydrocarbon decomposition.

Another key finding, consistent with expectation, is that the production of hydrogen initiates when the plasma ignites in the hydrocarbon-carrier gas mixture. The only lag time observed corresponds to the residence time that depends on the flow rate and the volume of the fluid flow system. For this microfluidic reactor and flow system, this lag is only on the order of seconds. Also consistent with expectation, the rate of production of hydrogen is proportionate to the power input to the plasma. This is illustrated in Fig. 3, which shows monotonic increases in hydrogen concentration in the outlet stream with increasing input power.

In order to understand the basic behavior of the microplasma reaction, we completed several experimental runs for the measurement of conversion and the concurrent consumption of electrical power. The determination of energy efficiency is a critical aspect for the evaluation of this reaction arrangement as a key element in a scheme for the production of electrical power from high energy density hydrocarbons. Although several experiments have been completed to date, we are still in an exploratory phase far from an optimal configuration that could allow for such an assessment. Consequently, we present here two experiments that illustrate the approach we have taken for closing the mass and energy balances of the system. Follow-up articles will present a more complete summary of the body of experiments at a later date.

The mass balance is performed based on knowledge of the input flow rates and the composition of the output flow obtained with the mass spectrometer and gas chromatograph. Fig. 4 shows the evolution of hydrogen and other products with the introduction

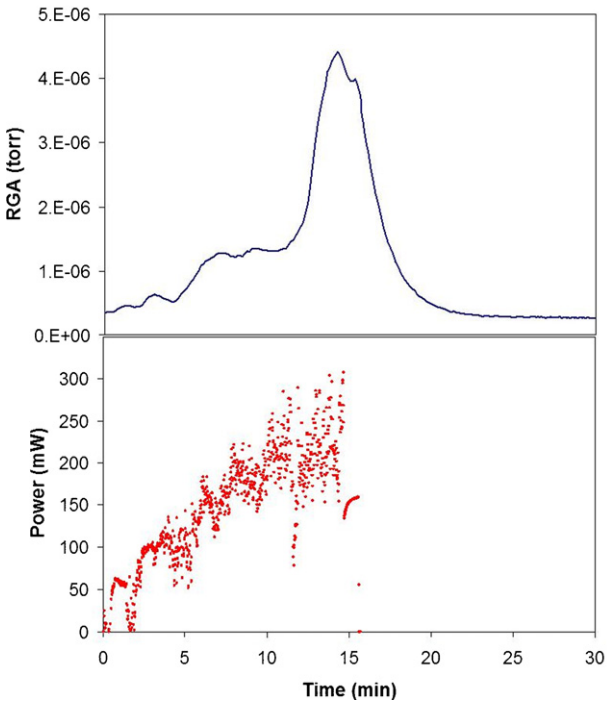

Fig. 3. Increase of hydrogen signal in mass spectrometer (upper) as DC power input to the microplasma reactor chip is increased (lower).

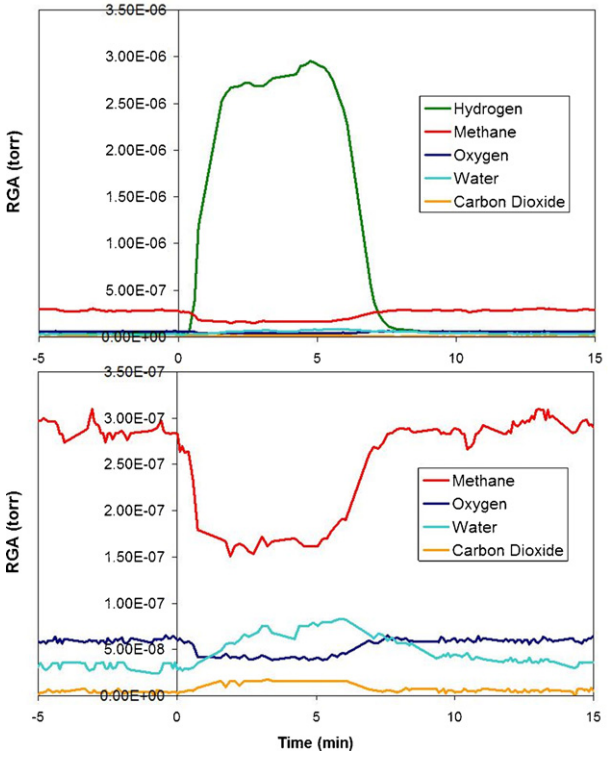

Fig. 4. Mass spectrum output for Experiment J15. Elevated hydrogen signal (upper) is coincident with depressed methane signal (lower). Production of water with depletion of residual oxygen signal is seen (lower). Trace production of CO_2 is observed during methane conversion interval (lower).

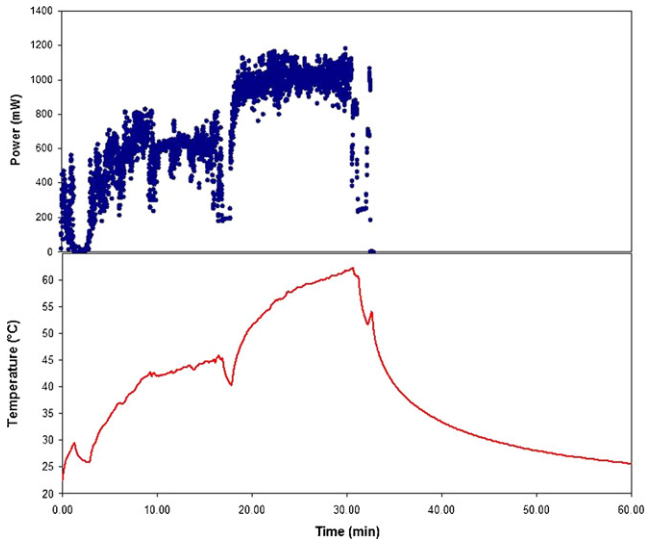

Fig. 5. DC power dissipation in the microplasma reactor (upper) during Experiment M25. Profile of temperature measured in situ by resistive thermal device mounted adjacent to chip on outlet side of channel (lower).

of plasma power. From this plot we see the consumption of the methane reactant and the concomitant production of hydrogen. Also visible is evidence of the low but finite rate of reaction of hydrogen product with residual oxygen to produce water, a reaction that is to be discouraged in the quest for the highest possible hydrogen yield.

Fig. 5 displays the system temperature during the course of a typical experiment (Experiment M25). From this plot we see that in this particular experiment the system does not reach thermal steady state, rather continuing to display an accumulation of energy by an increase in temperature. This storage rate is given by:

$$\frac{dE_{sys}}{dt} = (mC_p)_{sys}\frac{dT}{dt}, \tag{1}$$

where the mass, heat capacity, and temperature of the system, and time, are given their normal symbols. The plot also shows the cooling curve that is recorded after extinguishing the plasma. This curve provides information about heat loss rates since during cooling the storage term simply equals the heat loss term. The heat loss rate as a function of temperature determined from the cooling curve is then applied to the energy balance during the part of the experiment when the plasma is lit, and chemical reaction is occurring.

Table 1 summarizes the results of the mass balance for Experiment M25. The conditions of the experiment including gas flows,

Table 1
Mass balance for Experiment M25 based on feed gas flow rates and product distributions determined by gas chromatography and mass spectrometry. Methane and nitrogen were the feeds; residual oxygen is found in trace concentration in the feed.

	Experiment M25			
	Moles in (mmole)	Moles out (mmole)	Mass in (mg)	Mass out (mg)
N_2	3.31	3.31	92.8	92.8
CH_4	0.72	0.55	11.5	8.9
O_2	0.08	0.07	2.6	2.4
H_2	0.00	0.27	0.0	0.5
C_2H_2	0.00	0.02	0.0	0.5
H_20	0.00	0.02	0.0	0.3
C_2H_6	0.00	0.01	0.0	0.2
CO_2	0.00	0.00	0.0	0.0
C (s)	0.00	0.11	0.0	1.4
Total	4.11	4.36	106.9	106.9

Table 2
Summary of key process conditions, conversions, and energy balance rate terms for two representative experiments. Extent of non-closure of energy balance (12% for M25, 7% for J15) is of the same order as the uncertainty in energy rate measurements (≈15%). Energy quantities are quoted as energy rates in milliwatts. "% Enthalpy energy" is the ratio, expressed as a percentage, of enthalpy change due to chemical reaction to electrical energy input.

Experiment	M25	J15
Power supply	DC	Pulsed DC (15 kHz)
N_2 flow (seem)	2.27	2.27
CH_4 flow (seem)	0.46	0.13
Electrical energy (mW)	600	2500
Heat loss (mW)	325	700
Energy storage rate (mW)	205	1630
Reaction enthalpy (mW)	8.0	1.0
% Enthalpy energy	1.2%	0.04%
Conversion of CH_4	22.8%	41.3%
% H_2 in outlet	6.4%	3.8%

electrical power input, and power supply type, are indicated in Table 2. From the data in Table 1 we calculate hydrocarbon conversion as

$$X_{hc} = \frac{\dot{n}_{hc,i} - \dot{n}_{hc,f}}{\dot{n}_{hc,i}}, \tag{2}$$

where the $\dot{n}_{hc}$ represent the steady state molar flow rates of the hydrocarbon methane at the input and output.

The energy balance is determined by the well-established conservation equation [16]:

$$\sum_i \dot{E}_i - \sum_i \dot{E}_{out} = \frac{dE_{sys}}{dt}, \tag{3}$$

which is written in terms of energy rates. By inserting plasma power P_{in} as an energy input rate, and $\dot{Q}$ as the rate of heat input (which is always a negative quantity in our experiments, i.e., heat is released to the ambient), and the enthalpies of incoming and outgoing gas streams, we arrive at:

$$\sum_i (\dot{m}_i H_i) - \sum_i (\dot{m}_i H_i)_{out} + P_{in} + \dot{Q} = (mC_p)_{sys}\frac{dT}{dt}. \tag{4}$$

The first two terms represent an energy input rate and energy output rate, respectively, by virtue of the enthalpy H and mass flow rate $\dot{m}$ of each species in feed and product streams. The enthalpy includes the effects of temperature rise of products and unreacted feed species appearing in the output stream. Cases when the system temperature has reached steady state are most straightforward to analyze since the right hand side of Eq. (4) then becomes zero. However, many experiments fail to reach thermal steady state as illustrated by the constant rise of system temperature in Fig. 5.

We summarize the outcome of the mass and energy balances for two experiments in Table 2. The key differences between the experimental conditions are the following: (a) the reactant flow composition differed significantly: in J15 the hydrocarbon is much more dilute in the carrier than in M25, and (b) M25 was carried out with DC power whereas J15 utilized pulsed DC power. The power levels investigated in each differ as well. This was related to the changing accessibility of plasma conditions as flow settings are varied.

4. Discussion

The decomposition of methane reaction produces hydrogen and elemental carbon by:

$$CH_4 \rightarrow 2H_2 + C(s) \tag{5}$$

The reaction is endothermic with a standard heat of reaction of 74.9 kJ mol^{-1}. Increased input power to the plasma is expected

to have the effect of elevating the electron temperature, with the result that increased energy is available to reacting species. The result then is expected to be similar to elevating the temperature of an endothermic reaction in a conventional reactor, that is, the equilibrium conversion increases. The effect is observed in our data, namely that hydrogen production increases with increasing power level as illustrated in Fig. 3.

The effect that conversion [17,18] is enhanced by the presence of nitrogen or other carrier has been observed previously by several groups in different plasma configurations [19]. Dinitrogen has a significantly higher energy of dissociation than methane. In the case of high density atmospheric plasma it is believed that the reaction enhancement is mediated through excited N_2 molecules in higher vibrational and meta-stable states (see references in [19]) rather than via nitrogen ions or reactive neutrals, which may be effective in other situations [20,21].

The observation that air provides the same benefit as pure nitrogen in facilitating reaction would prove extremely beneficial in a practical system since no additional resources for carrier storage would be required. The low rates of oxidation even with the presence of oxygen in this scenario are remarkably attractive. Residual air carrier in the reformate stream would not be detrimental to leading fuel cell technologies except for the effect of dilution which impacts electrocatalytic reaction rate. Microplasma-based systems at higher scale could provide a separation subsystem (for example Pd membrane separation) to eliminate this effect if desired.

The tendency for the reaction to produce hydrogen without significant carbon dioxide in the effluent stream is an extremely attractive aspect of the process. Current hydrocarbon reforming schemes generally produce CO_2 as a byproduct which is considered unacceptable in light of growing environmental concern. Such schemes if implemented in the future must incorporate a CO_2 capture strategy, with the result that complexity and costs are added. Even biofuel implementation, considered to be net carbon neutral, produces CO_2. If CO_2-free microplasma reforming could be realized, it would be considered superior from a carbon management standpoint.

In reviewing the energy efficiency results, we observe utilization of input energy to effect chemical conversion at a relatively low level of less than 1% or so in the results shown in Table 2. It must be noted that the purpose of the experiments reported was to explore the feasibility of hydrocarbon reforming in a microplasma environment. No optimization has taken place of device geometries or processing conditions which could both lead to greater conversion, hydrogen production rate, and energy efficiency. For example, the use of pulsed DC appears to offer the possibility of greater conversion but apparently at the cost of greater expenditure of energy. Optimization of power supply frequency, duty cycle, etc. could be a fruitful line of research.

The energy budget broken down in Table 2 is similar to the results of a study carried out in a dielectric barrier discharge reactor in [22]. In our case, if the thermal losses to the environment could be reduced and effectively exploited for chemical conversion, energy efficiency could be improved. One approach to this would be to insulate the reactor against losses by convection and radiation to the ambient. Insulating the reactor would cause the temperature to rise without additional power input. Elevated temperature, as noted earlier in this section, will serve to increase the equilibrium conversion of the key endothermic reaction.

5. Conclusions

We conclude that the microplasma reactor shows promise for advanced catalyst-free reforming of hydrocarbons. While mass and energy balances are not yet favorable, optimization of device and process variables may yield significant improvements. The ability to process hydrocarbons with little or no CO_2 effluent is extremely attractive and may represent value for certain applications outside power generation, for example in specialized chemical synthesis.

Acknowledgements

The authors wish to acknowledge the assistance of Sang Youp Hwang in the laboratory experiments and data analysis. The support of George Wohlrab and Bruce Fraser for equipment fabrication is gratefully acknowledged. We acknowledge Army Research Office (grant W911NF-07-1-0118) for financial support of the project. This work was performed in part at the Cornell NanoScale Facility, a member of the National Nanotechnology Infrastructure Network, which is supported by the National Science Foundation (grant ECS-0335765). The support of the National Science Foundation under grant DGE-0742462 is gratefully acknowledged.

References

[1] J. Larminie, A. Dicks, Fuel Cell Systems Explained, second ed., Wiley, Hoboken, NJ, 2003.
[2] C. Song, Catal. Today 77 (2002) 17–49.
[3] K. Shah, R.S. Besser, J. Power Sources 166 (2007) 177–193.
[4] G. Kolb, J. Schürer, D. Tiemann, M. Wichert, R. Zapf, V. Hessel, H. Löwe, J. Power Sources 171 (2007) 198–204.
[5] K.H. Becker, K.H. Schoenbach, J.G. Eden, J. Phys. D: Appl. Phys. 39 (2006) R55.
[6] R. Foest, M. Schmidt, K. Becker, Int. J. Mass Spectrom. 248 (2006) 87–102.
[7] A. Koutsospyros, S.M. Yin, C. Christodoulatos, K. Becker, Int. J. Mass Spectrom. 233 (2004) 305–315.
[8] G. Petitpas, J.D. Rollier, A. Darmon, J. Gonzalez-Aguilar, R. Metkemeijer, L. Fulcheri, Int. J. Hydrogen Energy 32 (2007) 2848–2867.
[9] L. Bromberg, D.R. Cohn, A. Rabinovich, N. Alexeev, Int. J. Hydrogen Energy 24 (1999) 1131–1137.
[10] T. Paulmier, L. Fulcheri, Chem. Eng. J. 106 (2005) 59–71.
[11] H. Qiu, K. Martus, W.Y. Lee, K. Becker, Int. J. Mass Spectrom. 233 (2004) 19–24.
[12] G.J. Kim, Y.J. Hong, F. Iza, J.K. Lee, Comput. Phys. Commun. 177 (2007) 131.
[13] K.H. Schoenbach, R. Verhappen, T. Tessnow, F.E. Peterkin, W.W. Byszewski, Appl. Phys. Lett. 68 (1996) 13–15.
[14] P. Kurunczi, N. Abramzon, M. Figus, K. Becker, Acta Phys. Slovaca 54 (2004) 115–124.
[15] R.S. Besser, W.C. Shin, J. Vac. Sci. Technol. B: Microelectron. Nanometer Struct. 21 (2003) 912–915.
[16] H.S. Fogler, Elements of Chemical Reactor Engineering, fourth ed., Prentice-Hall, Upper Saddle River, NJ, 2006.
[17] J.C. Legrand, A.M. Diamy, R. Hrach, V. Hrachová, Vacuum 48 (1997) 671–675.
[18] A. Indarto, J.W. Choi, H. Lee, H.K. Song, J. Nat. Gas Chem. 14 (2005) 13–21.
[19] A. Indarto, J.W. Choi, H. Lee, H.K. Song, Energy 31 (2006) 2650–2659.
[20] A.M. Diamy, R. Hrach, V. Hrachova, J.C. Legrand, Vacuum 61 (2001) 403–407.
[21] S.Y. Savinov, H. Lee, H.K. Song, B.K. Na, Plasma Chem. Plasma Process. 23 (2003) 159–173.
[22] T. Nozaki, Y. Miyazaki, Y. Unno, K. Okazaki, J. Phys. D: Appl. Phys. 34 (2001) 3383–3390.